PCCP

Accepted Manuscript

This is an *Accepted Manuscript*, which has been through the Royal Society of Chemistry peer review process and has been accepted for publication.

Accepted Manuscripts are published online shortly after acceptance, before technical editing, formatting and proof reading. Using this free service, authors can make their results available to the community, in citable form, before we publish the edited article. We will replace this *Accepted Manuscript* with the edited and formatted *Advance Article* as soon as it is available.

You can find more information about *Accepted Manuscripts* in the Information for Authors.

Please note that technical editing may introduce minor changes to the text and/or graphics, which may alter content. The journal's standard Terms & Conditions and the Ethical guidelines still apply. In no event shall the Royal Society of Chemistry be held responsible for any errors or omissions in this *Accepted Manuscript* or any consequences arising from the use of any information it contains.

ROYAL SOCIETY OF CHEMISTRY

www.rsc.org/pccp

Physical Chemistry Chemical Physics RSCPublishing

PAPER

Influence of the interface in quantum corrections to low-temperature resistance of $La_{2/3}Sr_{1/3}MnO_3$ trilayer masking thin films

Cite this: DOI: 10.1039/x0xx00000x

Received 00th January 2012,
Accepted 00th January 2012

DOI: 10.1039/x0xx00000x

www.rsc.org/

Yuan Jin,[a] Xiao-Peng Cui,[a] Wei-Hua Han,[b] Shi-Xun Cao,[a] Yu-Ze Gao,[a] and Jin-Cang Zhang,[a,*]

We report the low-temperature resistance upturn in sandwiched structures of $La_{2/3}Sr_{1/3}MnO_3/ZrO_2/La_{2/3}Sr_{1/3}MnO_3$, $La_{2/3}Sr_{1/3}MnO_3/LaMnO_3/La_{2/3}Sr_{1/3}MnO_3$, while it disappeared when the interlayer was replaced by $YBa_2Cu_3O_7$. The experimental data have been analyzed qualitatively and quantitatively. The results show that the low temperature resistance upturn is mainly due to the quantum correction effects driven by the weak localization and the electron-electron interaction in such a strongly correlated system, and the contribution of each factor varies with grain boundaries. Meanwhile, the resistance upturns are suppressed by local magnetic field. These findings will help to further understand the physical mechanism of low-temperature resistance upturn in colossal magnetoresistance manganites. Furthermore, it is also helpful to reveal the intrinsic transport mechanism at the interfaces of semiconductor/ferromagnetism and antiferromagnetism/ferromagnetism.

Introduction

In the past decade, extensive work both experimental and theoretical has been performed, and several models have been built to interpret the low-temperature resistivity minima behavior in colossal magnetoresistance (CMR) manganites.[1-7] The observed phenomenon is similar to the Kondo effect, which was first found in the crystalline noble-metal alloys with low magnetic impurity concentration.[8] So far, in order to explain these interesting and abnormal phenomena in ferromagnetic (FM) metallic phase, various mechanisms have been proposed, such as spin-polarized tunneling through grain boundaries, Kondo-type effect due to spin disorder, and quantum correction effects. However, the low-temperature resistance minimum is still under debate due to the complexity of the manganite system. Reviewing these existing experimental results and theoretical explanations, Rozenberg *et al.*[9] and Auslender *et al.*[10] obtained a shallow minimum on ceramic $La_{0.5}Pb_{0.5}MnO_3$ and $La_{0.8}Sr_{0.2}MnO_3$ sample at the temperature of 25–30 K under zero magnetic field. The temperature for resistivity minima of Kondo effect, T_{min}, shifts towards lower temperatures under external magnetic fields and disappears at a certain field. They interpreted these phenomena with the quantum corrections to conductivity (QCC) model including electron-electron interaction and weak localization effect. The electron-electron interaction is the Coulomb scattering from one electron wave to another and the weak localization is a quantum correction due to the finite dimension of the system as quantum interference between backscatter waves and propagating waves.[11-12] Weak localization and weak anti-localization are quantum interference effects in a disordered electron system. Weak anti-localization arises from spin-orbit interaction and enhances the conductivity while weak localization suppresses the conductivity with decreasing temperature at very low temperatures.[13] weak localization and weak anti-localization have attracted a lot of attention in recent years.[13-15] Although much effort had been devoted to explaining the resistance upturn behavior in CMR manganites, but up to date, clear conclusion has not been drawn yet since there are too many different experimental phenomena and interpretations. Xu *et al.* [16] have investigated the behavior of the resistivity upturn of polycrystalline $La_{2/3}Ca_{1/3}MnO_3$ (LCMO) under various magnetic fields at low temperature. They found that such a behavior would be suppressed and then become independent of the magnetic field when the magnetic field is higher than 1 T. Jia *et al.*[17] have grown single-crystal of $La_{2/3}Sr_{1/3}MnO_3$ (LSMO) in oxygen-sufficient condition, and showed that the low-temperature resistivity minima disappeared in magnetically homogeneous LSMO single-crystal. It implies that low-temperature resistivity upturn behavior should have correlation with the contribution of grain boundary. Then, Jia *et al.*[18] investigated the effects of the ferroelectric poling-induced strain on the sputtered $La_{0.7}Ca_{0.15}Sr_{0.15}MnO_3$ films grown on poled ferroelectric single-crystal substrates. The ferroelectric poling will induce a reduction of the in-plane tensile strain and thus the lattice distortion, which suppresses the resistivity upturn. Previously,[19] we have fabricated granular films, ZrO_2 precipitated on LSMO films, and discovered that the low-temperature resistivity upturn behaviors can be enhanced by increasing the precipitate concentration of ZrO_2. In other words, the low-temperature resistivity upturn behaviors can be modulated by the interfaces or grain boundaries between LSMO and the second phase precipitates. We also investigated

Physical Chemistry Chemical Physics Accepted Manuscript

single layer LSMO thin films, it still exist the resistance upturn at low temperature, while the resistance upturns are hardly affected by the applied magnetic fields.[19]

Thus, in order to further investigate the effects of grain boundaries on the low-temperature resistance upturn transports in CMR manganites, we fabricated trilayer masking epitaxial thin films along with different interfaces to simulate grain boundaries which make defects in LSMO and induce scattering and backscattering, there are two kinds of grain boundaries: normal grain boundary and phase separation domain boundary.[20-24] We choose the FM metallic LSMO, which not only shows the highest Curie temperature (T_C ~ 370 K), but also exhibits almost 100% spin polarization and the largest single electron bandwidth,[25-28] and the relation with electrical transport which gives a bright future in the applications,[29-34] as both the cap and the bottom layers, along with three different kinds of spacer layers for grain boundaries, the stabilized nonmagnetic semiconductor Zirconia spacer for the normal grain boundary,[35] antiferromagnetic (AFM) insulator $LaMnO_3$ (LMO) spacer for the FM/AFM phase separation domain boundary of LSMO layers,[36] and *high-T_c* superconductor (SC) $YBa_2Cu_3O_7$ (YBCO) spacer for comparison, because the YBCO is superconductive at low temperature, it will benefit the resistance induced by bilayer LSMO at low temperature.[37] Meanwhile, the magnetotransport properties were measured by vertical resistance measurement with the applied magnetic fields H perpendicular to the plane of the masking film. In this work, the low-temperature resistance upturns were found in LSMO/ZrO_2/LSMO and LSMO/LMO/LSMO, but it disappeared in LSMO/YBCO/LSMO. The correlation of the interfaces between LSMO and different intermediate spacer on low-temperature resistance upturns was systemically analyzed by qualitative and quantitative analysis method. The results proved that the grain boundary will dominate the low-temperature abnormal transport behaviors, and the electron-electron interaction is hardly affected by the magnetic field or the spacer, while weak localization is sensitive to the magnetic field and the spacer.[38-39] It is remarkable that the interfaces will tune the quantum corrections to resistance. Moreover, our results proved that the grain boundary will induce the quantum correction to resistance and lead to the low-temperature resistance upturn.

Experimental

The manganite targets composite of LSMO were prepared by the standard solid-state reaction method. It was prepared by mixing the heat treating stoichiometric quantities of high purity La_2O_3, $SrCO_3$, and MnO_2, the raw materials were mixed, palletized and sintered at 1000 ℃ for 12 h, 1200 ℃ for 24 h and 1350 ℃ for 24 h with intimately intermediate grinding and repelletizing. At the same time, the target of ZrO_2 was chosen by nanoparticle ZrO_2 material then palletized and sintered at 1000 ℃ for 12 h. The target of LMO was prepared by mixing the heat treating stoichiometric quantities of high purity La_2O_3 and MnO_2, the raw materials were mixed, palletized and sintered at 1000 ℃ for 12 h, 1200 ℃ for 24 h and 1350 ℃ for 24 h with intimately intermediate grinding and repelletizing. The target of YBCO were prepared by heat treating stoichiometric quantities of high purity Y_2O_3, $BaCO_3$, and CuO powders at 950 ℃ for 20 h in oxygen atmosphere. The heat treatment was repeated twice after grinding and repelletizing each time to ensure the homogeneity of the samples.

We have fabricated three kinds of trilayer masking film samples, LSMO/ZrO_2/LSMO, LSMO/LMO/LSMO, and LSMO/YBCO/LSMO. A standard pulsed laser deposited (PLD) techniques equipped with multiple targets and KrF excimer laser (λ = 248 nm) was used to grow the trilayer masking films on the substrates of 5 × 3 × 0.5 mm^3 single-crystal (100)-oriented $LaAlO_3$ (LAO). Laser deposition process applying the following parameters: repetition rate 2 Hz, pulsed laser energy density was around 1.6 J /cm^2, deposition temperature 770 ℃, and oxygen pressure 0.4 mbar. During the deposition procedure, a 50 nm LSMO epitaxial layer as the bottom layer was deposited firstly on (100) LAO substrate and annealed for 30 minutes, then cooled down to room temperature in the chamber. A mask was used to partially covered the surface and selectively deposited the barrier materials, which represents 6 unit cell thick nonmagnetic ZrO_2 (c = 5.147 Å; ~3 nm), AFM LMO (c = 7.699 Å; ~5 nm) the same 6 unit cell thick as ZrO_2 layer, or 25 unit cell thick YBCO (~30 nm), were deposited on the pre-deposited LSMO layers, respectively. A 30 nm-thick spacer of YBCO was used to avoid the magnetic fluctuations which occur within a correlation length of 12 unit cell ≈ 14 nm in the normal phase of YBCO in FM/SC bilayers.[40] After that, another 50 nm cap LSMO layer was deposited onto the intermediate spacer. Barrier materials and cap LSMO were prepared under the same conditions. After deposition, the trilayer masking films were cooled to room temperature and post-annealed under 1 atm of flowing O_2 at 630 ℃ for 30 minutes. The electrical resistance was measured using four stripe contacts on unpatterned samples with evaporated chromium/gold (20 nm/200 nm) pads as current and voltage probes. In order to get the nice vertical transport across the spacer layer and reduce/avoid the lateral transport across the two central pads, the distance of the central pads were made much close (0.5 mm).

The X-ray diffraction (XRD, 18kWD/max-2550 model, Cu *Ka* radiation) was used to qualify the films at room temperature in the 2θ range of 20°-80 °with a step of 0.02 °. The crystallinity and texture were characterized by XRD spectra with the aid of JADE 6.0 software. The surface topography is detected by an Optical Microscope. All the measurements were performed on the same samples. Electrical and magnetic measurements were carried out using the Physical Property Measurement System (PPMS-9) and Superconducting Quantum Interference Device (SQUID) (Quantum Design). Electrical transport measurements were carried out with Gold wires as electrical leads and using the standard dc four-probe technique in the temperature range from 3-380 K under dc magnetic fields between 0 and 6.0 T perpendicular to the film plane.

Results and discussion

Fig. 1(a) depicts the XRD patterns for LSMO/ZrO_2/LSMO and LSMO/YBCO/LSMO. The heterostures with a ZrO_2 spacer and YBCO spacer in addition to the (100) LAO substrate peaks only (*h*00) peaks from LSMO. From the XRD patterns, we can conclude that the peaks of our samples are very sharp and no visible impurities peaks. Meanwhile, Fig. 1(b) presents the Optical Microscope picture of the trilayer masking thin film. The light-colored section in the right is the single layer LSMO, and the dark part in the left is the trilayer heterostructure, yellow and shining sheets in the pictures are the chromium/gold pads. It is evident that the film has a smooth surface and the boundary between single layer and trilayer heterostructure is very clear. Fig. 1(c) illustrates the schematic sketch of FM/spacer/FM heterostructure, the green blocks are LSMO and the red block presents the spacer, yellow sheets in the figure are the chromium/gold current and voltage probe pads.

Physical Chemistry Chemical Physics Accepted Manuscript

 This journal is © The Royal Society of Chemistry 2012

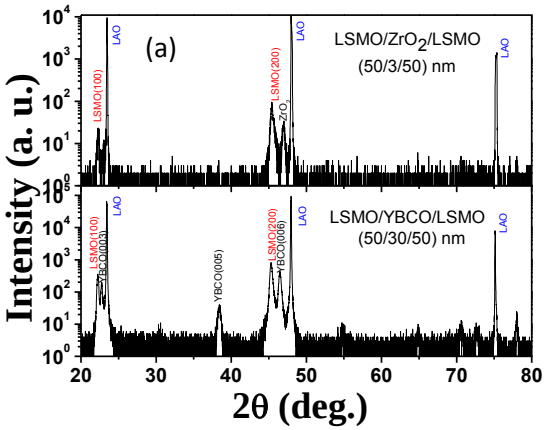

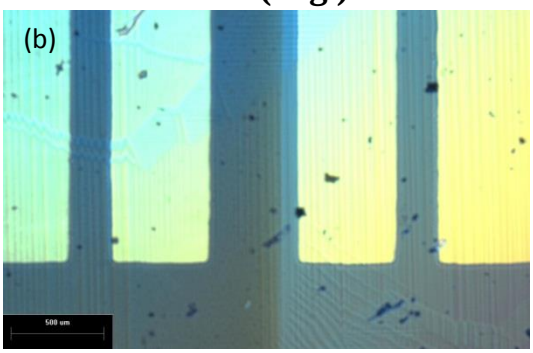

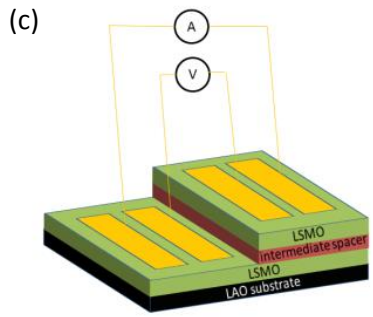

Fig. 1 (a) X-ray diffractioin pattern for LSMO/ZrO_2/LSMO and LSMO/YBCO/LSMO. (b) Optical microscope image for the surface of the LSMO/YBCO/LSMO. (c) Schematic sketch of FM/spacer/FM masking heterostructure, the bottom black part presents the LAO substrate.

Fig. 2 shows the whole range of 3-380 K resistance under zero and various applied magnetic fields for the three samples. Samples were cooled from 380 K to 3 K, then the resistance was measured from 3 to 380 K during the warming process; the magnetic field was applied throughout the cooling and warming processes. The temperature dependence of magnetotransport properties for LSMO/ZrO_2/LSMO film is presented in Fig. 2(a), it can be seen that the metal-semiconductor transition occurs slowly increase with the magnetic field increases, which means double exchange of LSMO do work in the system. The double exchange model of Zener and a strong electron-phonon interaction arising from the *Jahn-Teller* splitting of Mn *d* levels explained most of the electrical and magnetic properties of LSMO manganites.[25, 41] Moreover, it shows strong dependence on the applied fields *H* which indicates the colossal magnetoresistance effect exists in our sample. In the inset of Fig. 2(a), a normalized resistivity is used by $\Delta R = R(T) / R(T = 60\ K)$. It can be seen that all of distinct resistance minima R_{min} under various applied fields appear at 15 K. Meanwhile, Fig. 2(b) presents the temperature dependence of the magnetotransport properties for the LSMO/LMO/LSMO heterostructure with the antiferromagnetic insulator LMO spacer. Like LSMO/ZrO_2/LSMO, the metal-semiconductor transition slowly increases with the applied field increases and the magnetoresistance effect also exists in our sample which all can be ascribed to double exchange. Unlike Zirconia spacer which presents normal grain boundary of cap and bottom LSMO layers, the LMO spacer of the heterostructure can be considered as the FM/AFM phase separation domain boundary of cap and bottom LSMO layers. Meanwhile, the applied magnetic fields always parallel to the spin of Mn t_{2g} local electrons and promote the double exchange motion of Mn e_g electrons, and in LSMO/LMO/LSMO heterostructure, LMO layer can provide Mn e_g itinerant electrons. The resistance minimum R_{min} also appears all nearly at 13 K under various applied fields from 0 to 6 T at the low-temperature region from 3 to 25 K in the inset of Fig. 2(b). However, the resistance upturns under various applied fields disappear in LSMO/YBCO/LSMO heterostructure which is presented in Fig. 2(c). Comparing to our previous research,[19, 42] we can conclude that YBCO can compensate the contribution of electron-electron interaction. That reveals the disappearance reason of the resistance upturn in YBCO intermediate spacer system.

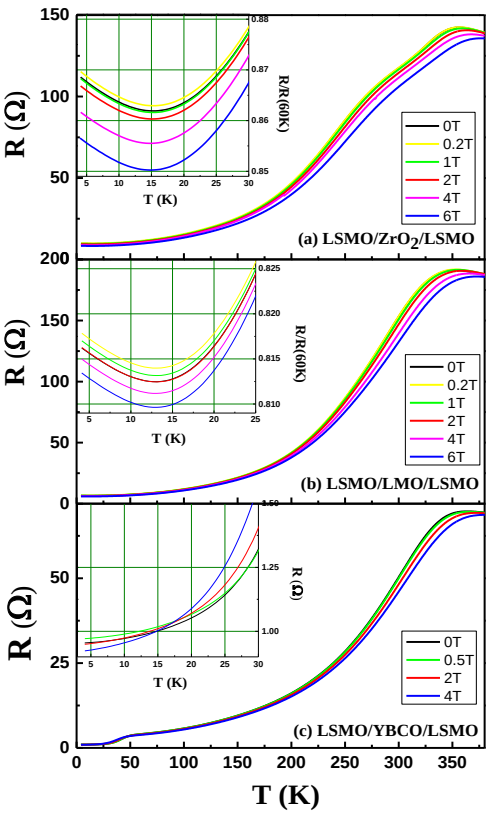

Fig. 2 Temperature dependence of the electrical transport properties for (a) LSMO/ZrO_2/LSMO, (b) LSMO/LMO/LSMO, and (c) LSMO/YBCO/LSMO measured under various magnetic fields. Inset presents the low-temperature extended scale from 3 – 30 K.

Physical Chemistry Chemical Physics Accepted Manuscript

In order to investigate the influence of nonmagnetic ZrO_2 spacer and AFM LMO spacer on the observed resistance upturn in LSMO heterostructures, qualitative analysis is firstly used. It is well known that, the contribution of weak localization would be suppressed by a strong magnetic field.[16, 18] From this point, a disentanglement of the contributions can be accomplished if we make use of the effect that a strong magnetic field suppresses the contribution of weak localization. Fig. 3 plots the depth of resistance upturn data $\Delta R = R(T) - R_{min}$ for different applied magnetic fields as a function of temperature. It turns out that the values for R_{min} do not depend on the temperature. The data are separated into two parts. The first part ΔR_1 is the attribute in the difference between resistance at 0 T and resistance under a strong magnetic field $\Delta R_1(T) = R_{0T}(T) - R_{6T}(T)$ for the field-dependent part which directly related to the contribution of weak localization. The second part is the depth $\Delta R_2(T) = R_{6T}(T) - R_{6T\ min}$ for the field-independent part which is induced by electron-electron interaction and have no reference to the applied magnetic fields. In Fig. 3(a) and Fig. 3(b), $\Delta R_{2\ (LMO)}$ nearly equals to $\Delta R_{2\ (ZrO2)}$, but $\Delta R_{1\ (LMO)}$ is much smaller than $\Delta R_{1\ (ZrO2)}$, which indicate that the contribution of weak localization are suppressed more by the interface of LSMO/ZrO_2 than LSMO/LMO. While compared with 54 nm pure LSMO thin film data, the resistance upturns still exist at low temperature, but they are hardly affected by the applied magnetic fields, $\Delta R_{1\ (LSMO)} = 1.214 \times 10^{-6} \approx 0$, which has no grain boundary or interface in the thin single-crystal film, so no contribution to weak localization.[19]

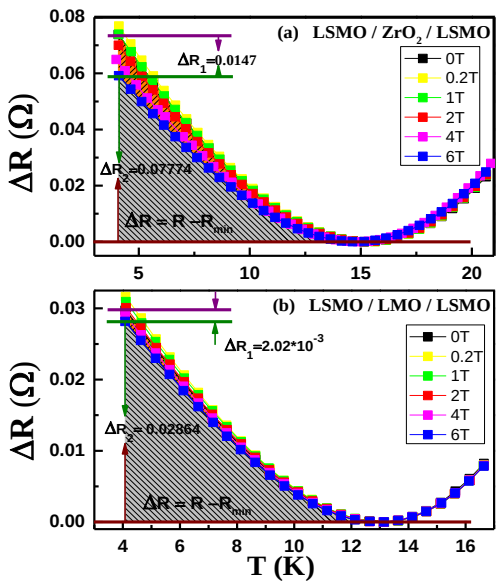

Fig. 3 $\Delta R = R(T) - R_{min}$ as a function of temperature for (a) LSMO/ZrO_2/LSMO and (b) LSMO/LMO/LSMO trilayer thin films. The first part (orange) $\Delta R_1(T) = R_{0T}(T) - R_{6T}(T)$ is the attribute for the field-dependent part; the second part (grey) $\Delta R_2(T) = R_{6T}(T) - R_{6T\ min}$ is the field-independent part.

After qualitative analysis, quantitative analysis needs to be analyzed for the experimental data. At first, we considered the magnetic based Kondo scattering which gives rise to a form of $R \propto lnT$ and dominates the low-temperature resistance upturn behavior, so we fitted our experimental data using Kondo scattering form, but failed. Consequently, the possibility of Kondo contribution to the upturn can be excluded. Meanwhile, the data shows unchanged T_{min} in a magnetic field also can rule out Kondo scattering effect. Then, the analysis of the data within the frame of the electron-electron interaction and weak localization are taken into account. In general, the total depth of low-temperature resistance in the first-order correction can be given by the following expression:

$$R = R_0 + R_m(T, H) - R_0^2[\sigma_{ee}(T, H) + \sigma_{wl}(T, H)] + R_{ep}(T), \quad (1)$$

where the $R_m(T, H)$ is the magnetic resistance contributed from the anisotropic MR and magnon scattering.

Based on the strong correlated effect in manganites, the conductivity of the e-e interaction which insensitive to the applied magnetic field can be described as,[9, 43]

$$\sigma_{ee}(T, H) = \sigma_0 + 0.0309\frac{e^2}{\hbar L_T}, \quad (2)$$

where $L_T^{-1} = \sqrt{k_B T/\hbar D} = \beta\sqrt{T}$ is the diffusion length of thermally excited carriers and D is the carrier diffusion constant. Then, according to the theory of Ziese[11] and Lee[43], the formula for conductivity correction due to contribution of weak localization is,

$$\sigma_{wl}(T, H) = \sigma_0 + \frac{e^2}{\hbar(2\pi)^2}(L_H + lnL_\varphi), \quad (3)$$

where $L_H = \sqrt{\hbar c/eH}$ is the magnetic length, and L_φ is the phase relaxation length due to Coulomb interaction has been obtained by E. Rozenberg et al.[9] and M. Auslender et al.[10] given by $L_\varphi^{-2} = \frac{\gamma e^2}{\hbar} L_T^{-3}$.

Therefore, the total resistivity at these temperatures can be represented can be expressed as,

$$R(T, H) = \frac{1}{\sigma_0 + a(H)lnT} - \beta T^{1/2} + pT^5 \quad (4)$$

The first term corresponding to the weak localization is considered together in 2D theory,[38, 44] and it will be suppressed by high magnetic field, the parameter $\alpha(H)$ is field-dependent,[16] σ_0 is the free fitting parameters.[45] The second term describes the contribution of electron-electron interaction in 3D theory for LSMO which is a strong correlated system,[9-10, 43] and it is hardly affected by the magnetic field. Considering the temperature range discussed here is far below Debye temperature, the third term is due to the electron-phonon interaction which takes the form $R_{ep} = pT^5$ and independent with magnetic field.[46] The intermediate spacer (ZrO_2/LMO) contributes weak localization at low temperature.

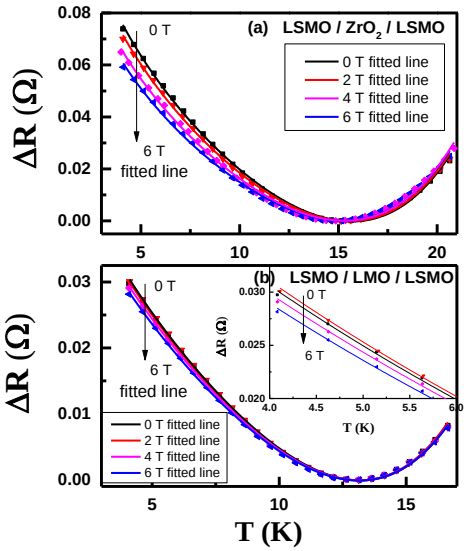

Fig. 4 Fit of ΔR data under 0T, 2T, 4T, and 6T applied fields using Eq. (4) for (a) LSMO/ZrO_2/LSMO and (b) LSMO/LMO/LSMO trilayer thin films, inset of (b) shows the extended scale of fitted line for LSMO/LMO/LSMO.

Physical Chemistry Chemical Physics Accepted Manuscript

This journal is © The Royal Society of Chemistry 2012

For Drude formula $\sigma = ne^2\tau/m^* = ne^2l\lambda_F/h$, with $n \approx 10^{28}$ m^{-3}, the Fermi wavelength of LSMO $\lambda_F \approx 0.35$ nm,[47] and depending on our previous research,[19] the ~50nm thickness pure LSMO thin film experimental value of σ is $\sigma \approx 7.7 \times 10^5\ \Omega^{-1}$m^{-1} at 2 K, yielding the mean free path l to be $l \approx 5.7$ nm. The spacer is insulating and the thickness is ~3 or 5 nm. The density of carriers which depending on the tunneling current is very low, the mean free path is far large the thickness of the intermediate. So we fitted the weak localization in 2D theory ($\sim lnT$).[38, 44] While the contribution of electron-electron interaction induces by LSMO which is a strong correlated system. As the pure LSMO mean free path is $l \approx 5.7$ nm, and the thickness of LSMO is 50 nm which is much larger than the mean free path. This system should belong to 3D in electron-electron interaction. We fitted the electron-electron interaction using the 3D theory ($\sim T^{1/2}$).[9-10, 43]

We fitted our experimental data using Eq. (4), the fitted results of ΔR under 0 T, 2 T, 4 T, and 6 T field are shown in Fig. 4, the symbols are the experimental data and the solid lines are the fitting result. It is seen that the data are fitted perfectly and the values of the fitting parameters obtained are shown in Table 1. The error estimates χ^2 values of the fitting parameters are less than 0.01%, which indicates a good fitting using Eq. (4). Good fit represent weak localization and electron-electron interaction as the dominant mechanism yielding the resistance upturn in LSMO/ZrO_2/LSMO and LSMO/LMO/LSMO trilayer masking film, respectively. In LSMO/ZrO_2/LSMO, it is shown that the weak localization parameter α is positive, meanwhile, it increases with the increase of field represent that the contribution of weak localization is suppressed by the applied field. For LSMO/ZrO_2 interfaces, large lattice mismatch between LSMO and ZrO_2 which will induce a potential barrier or large normal grain boundary to the carriers. The grain boundaries can cause defects and distortions of LSMO, the defects and distortions will induce scattering and backscattering which make weak localization happen, hence, the resistance upturns behavior becomes more apparent. Consequently, it reflects that the weak localization in LSMO/ZrO_2/LSMO exists and dominates the resistance upturn, while it is suppressed by the applied magnetic fields.

Table 1 The fitting results of the parameters of Eq. (4) for LSMO/ZrO_2/LSMO and LSMO/LMO/LSMO trilayer thin films.

	H (T)	σ_0	β	α	$p\times10^{-8}$
LSMO/ZrO_2/LSMO	0.0	5.37219	0.03478	1.05999	1.78299
	2.0	5.64878	0.03327	1.10851	1.76445
	4.0	6.14083	0.03063	1.23253	1.74732
	6.0	6.51673	0.02848	1.37432	1.67453
LSMO/LMO/LSMO	0.0	12.61956	0.02465	-0.07472	2.24669
	2.0	12.50542	0.02448	-0.00104	2.21098
	4.0	12.94058	0.02428	-0.1339	2.18232
	6.0	13.3173	0.02368	-0.14928	2.14474

However, in LSMO/LMO/LSMO, all of the weak localization parameters α are negative and small, which means that the weak anti-localization in the LSMO/LMO interfaces is operative and enhances the conductivity. While most of the magnetic field dependent phenomena arise for the magnetic nature of LSMO and any signatures of localization effects and anti-localization effects are small contributions. Moreover, the interfaces between LSMO/LMO can be considered as FM/AFM phase separation domain boundaries, the AFM domain will scatter the tunneling of the spin-polarized carriers in FM domain of LSMO and consequently decrease the electron diffusion constant D which is directly related to the electron-electron interaction. Meanwhile, LMO and LSMO are parts of the strongly correlated electron system, so that the electron-electron interaction cannot be ignored. And from Table 1, the slight change of electron-electron interaction parameter β for LSMO/LMO/LSMO under the increase of magnetic fields is due to the small variation of the electron density of state at the Fermi surface $N(E_F)$ in the system. Thus, it reveals that the electron-electron interaction in LSMO/LMO/LSMO dominates the resistance upturn behaviors.

Therefore, our results clarified that the weak localization enhanced by ZrO_2 spacer is a crucial factor for the low-temperature resistance upturn in LSMO/ZrO_2/LSMO trilayer masking film, while the electron-electron interaction dominant this behavior in LSMO/LMO/LSMO trilayer masking film. Certainly, the quantitative analysis in Fig. 4 is in agreement with qualitative analysis in Fig. 3 as well.

Conclusions

In summary, the behavior of the resistance minimum and its dependence on magnetic fields at low temperatures is studied on the LSMO/ZrO_2/LSMO, LSMO/LMO/LSMO, and LSMO/YBCO/LSMO trilayer masking thin films. The resistance upturns take place on LSMO/ZrO_2/LSMO and LSMO/LMO/LSMO trilayer thin films. Accordingly, the experimental data have been analyzed by qualitative analysis and quantitative analysis to understand the influence of normal grain boundary ZrO_2 spacer and phase separation domain boundary LMO spacer on the FM metallic state LSMO thin films. In qualitative analysis, by observing the depth of resistance upturn data ΔR for different applied magnetic fields as a function of temperature, the contribution of weak localization which is field-dependent in LSMO/ZrO_2/LSMO is much stronger than LSMO/LMO/LSMO. Then, in quantitative analysis, by fitting the experimental data with theory combined with two factors: weak localization and electron-electron interaction. Our results prove that the weak localization is a crucial factor for the resistance upturn in LSMO/ZrO_2/LSMO at low temperature, while electron-electron interaction dominates this abnormal electrical transport upturn in LSMO/LMO/LSMO. The superconductor YBCO spacer will compensate the contribution of weak localization and electron-electron interaction.

Acknowledgements

This work was supported by the National Key Basic Research Program of China (Grant No. 2015CB921600), the National

Physical Chemistry Chemical Physics Accepted Manuscript

Natural Science Foundation of China (NSFC, Grants No. 51372149, No. 50932003, and No. 11274222), Shanghai Academy of Materials Genome Initiative (Project No. 14DZ2261200), Shanghai Pujiang Program (13PJD015) and Science & Technology commission of Shanghai Municipality (13ZR1415200), the Science and Technology Innovation Fund of the Shanghai Education Committee (No.12ZZ097). Experiments are partially supported from Max Planck Institute for Solid State Research, Analysis & Measurement Center and Laboratory for Microstructures of Shanghai University.

Notes and references

[a] *Materials Genome Institute and College of Science, Shanghai University, Shanghai 200444, China.* Fax/Tel: +86-21-66161146; E-mail: jczhang@shu.edu.cn.

[b] *School of Physical Science and Technology, Lanzhou University, Lanzhou 730000, China*

1 J. C. Zhang, Y. Xu, S. X. Cao, G. X. Cao, Y. F. Zhang, and C. Jing, *Phys. Rev. B: Condens. Matter Mater. Phys.*, 2005, **72,** 054410.
2 S. Stølen, E. Bakkenw and C. E. Mohn, *Phys. Chem. Chem. Phys.*, 2006, **8**, 429–447.
3 T. Z. Ward, Z. Gai, X. Y. Xu, H. W. Guo, L. F. Yin, and J. Shen, *Phys. Rev. Lett.*, 2011, **106**, 157207.
4 Y. H. Huang, C. H. Yan, S. Wang, F. Luo, Z. M. Wang, C. S. Liao, and G. X. Xu, *J. Mater. Chem.*, 2001, **11**, 3296–3299.
5 A. Caneschi, D. Gatteschi and R. Sessoli, *J. Chem. Soc., Dalton Trans.*, 1997, **21**, 3963–3970.
6 C. Beekman, J. Zaanen, and J. Aarts, *Phys. Rev. B: Condens. Matter Mater. Phys.*, 2011, **83,** 235128.
7 T. Kubo, Y. Tokura and S. Tarucha, *Phys. Rev. B: Condens. Matter Mater. Phys.*, 2011, **83,**115310.
8 J. Kondo, *Prog. Theo. Phys.*, 1964, **32**, 37-49.
9 E. Rozenberg, M. Auslender, I. Felner, and G.Gorodetsky, *J. Appl. Phys.*, 2000, **88**, 2578.
10 M. Auslender, A. E. Karkin, E. Rozenberg, and G. Gorodetsky, *J. Appl. Phys.*, 2001, **89**, 6639.
11 M. Ziese, *Phys. Rev. B: Condens. Matter Mater. Phys.*, 2003, **68**, 132411.
12 S. Hikami, A. I. Larkin, and Y. Nagaoka, *Prog. Theor. Phys.*, 1980, **63**, 707-710.
13 C. He, T. D. Sanders, M. T. Gray, F. J. Wong, V. V. Mehta, and Y. Suzuki, *Phys. Rev. B: Condens. Matter Mater. Phys.*, 2012, **86**, 081401(R).
14 G. L. Chen, J. Han, T. T. Huang, S. Datta, and D. B. Janes, *Phys. Rev. B: Condens. Matter Mater. Phys.*, 1993, **47**, 4084(R).
15 H. Wang, H. Liu, C. Z. Chang, H. Zuo, Y. Zhao, Y. Sun, Z. Xia, K He, X. Ma, X. C. Xie, Q. K. Xue, and J. Wang, *Sci. Rep.*, 2014, **4**, 5817.
16 Y. Xu, J. C. Zhang, G. X. Cao, C. Jing, and S. X. Cao, *Phys. Rev. B: Condens. Matter Mater. Phys.*, 2006, **73**, 224410.
17 R. R. Jia, Z. J. Feng, S. P. Wang, Y. S. Liu, C. Jing, S. X. Cao, and J. C. Zhang, *J. Cryst. Growth*, 2010, **312**, 1963.
18 R. R. Jia, J. C. Zhang, R. K. Zheng, D. M. Deng, H. U. Habermeier, H. L. Chan W., H. S. Luo, and S. X. Cao, *Phys. Rev. B: Condens. Matter Mater. Phys.*, 2010, **82**, 104418.
19 Y. Z. Gao, G. X. Cao, J. C. Zhang, and H. U. Habermeier, *Phys. Rev. B: Condens. Matter Mater. Phys.*, 2012, **85**, 195128.
20 Q. Lu, C. C. Chen, A. de Lozanne, *Science*, 1997, **276**, 2006-2008.
21 A. Machida, Y. Moritomo, E. Nishibori, M. Takata, M. Sakata, K. Ohoyama, S. Mori, N. Yamamoto, and A. Nakamura, *Phys. Rev. B: Condens. Matter Mater. Phys.*, 2000, **62**, 3883-3887.
22 D. D. Sarma, D. Topwal, U. Manju, S. R. Krishnakumar, M. Bertolo, S. La Rosa, G. Cautero, T. Y. Koo, P. A. Sharma, S. W. Cheong, and A. Fujimori, *Phys. Rev. Lett.*, 2004, **93**, 097202.
23 T. Becker, C. Streng, Y. Luo, V. Moshnyaga, B. Damaschke, N. Shannon, and K. Samwer, *Phys. Rev. Lett.*, 2002, **89**, 237203.
24 T. Zhang, X. P. Wang, and Q. F. Fang, *J. Phys. Chem. C*, 2011, **115**, 19482–19487.
25 C. Zener, *Phys. Rev.*, 1951, **81**, 440.
26 Y. Tokura, N. Nagaosa, *Science*, 2000, **288**, 462-468.
27 M. B. Salamon and M. Jaime, *Rev. Mod. Phys.*, 2001, **73**, 583-628.
28 H. Y. Hwang, S. -W. Cheong, N. P. Ong, and B. Batlogg, *Phys. Rev. Lett.*, 1996, **77**, 2041.
29 Z. H. Zeng, F. Calle-Vallejo, M. B. Mogensenc and J. Rossmeisl, *Phys. Chem. Chem. Phys.*, 2013, **15**, 7526-7533.
30 S. A. Wolf, D. D. Awschalom, R. A. Buhrman, J. M. Daughton, S. von Molnar, M. L. Roukes, A. Y. Chtchelkanova and D. M. Treger, *Science*, 2001, **294**, 1488.
31 J. Zeng and K. Q. Chen, *J. Mater. Chem. C*, 2013, **1**, 4014–4019.
32 R. A. De Souza, M. S. Islamb and E. Ivers-TiVe, *J. Mater. Chem.*, 1999, **9**, 1621–1627.
33 X. H. Zhu, Z. G. Liu, and N. B. Ming, *J. Mater. Chem.*, 2010, **20**, 4015–4030.
34 Y. Tian, S. R. Bakaul and T. Wu, *Nanoscale*, 2012, **4**, 1529–1540.
35 Z. D. Xu, L. N. Yu, X. G. Xu, J. Miao, and Y. Jiang, *Appl. Phys. Lett.*, 2014, 104, 192903.
36 E. Dagotto, *New J. Phys.*, 2005, **7**, 67.
37 J. Orenstein, A. J. Millis, *Science*, 2000, **288**, 468-474.
38 R. Scherwitzl, S. Gariglio, M. Gabay, P. Zubko, M. Gibert, and J. -M. Triscone, *Phys. Rev. Lett.*, 2011, **106**, 246403.
39 G. Bergmann, *Phys. Rep.*, 1984, **107**, 1-58.
40 J. Hoppler, J. Stahn, Ch. Niedermayer, V. K. Malik, H. Bouyanfif, A. J. Drew, M. Rössle, A. Buzdin, G. Cristiani, H. U. Habermeier, B. Keimer, and C. Bernhard, *Nat. Mater.*, 2009, **8**, 315-319.
41 V. Garcia, M. Bibes, A. Barthelemy, M. Bowen, E. Jacquet, J. P. Contour, and A. Fert, *Phys. Rev. B: Condens. Matter Mater. Phys.*, 2004, 69, 052403.
42 X. C. Yao, Y. Jin, M. T. Li, Zhe Li, G. X. Cao, S. X. Cao, and J. C. Zhang, *J. Alloys and Compd.*, 2011, **509**, 5472–5476.
43 P. A. Lee and T. V. Ramakrishnan, *Rev. Mod. Phys.*, 1985, **57**, 287.
44 L. Maritato, C. Adamo, C. Barone, G. M. De Luca, A. Galdi, P. Orgiani, and A. Yu. Petrov, *Phys. Rev. B: Condens. Matter Mater. Phys.*, 2006, **73**, 094456.
45 Y. Jin, X. L. Qian, B. Lu, S. X. Cao, and J. C. Zhang, *RSC Adv.*, 2015, **5**, 2354-2359.
46 J. Bass, W. P. Pratt, Jr., and P. A. Schroeder, *Rev. Mod. Phys.*, 1990, **62**, 645.
47 A. M. Haghiri-Gosnet, M. Koubaa, A. F. Santander-Syro, R. P. S. M. Lobo, Ph. Lecoeur, and B. Mercey, *Phys. Rev. B: Condens. Matter Mater. Phys.*, 2008, **78**, 115118.

Physical Chemistry Chemical Physics Accepted Manuscript

 This journal is © The Royal Society of Chemistry 2012